Development and confirmation of a simple procedure to measure solids distribution in fluidized beds using tracer particles

Yupeng Xu, Tingwen Li, Liqiang Lu, Xi Gao, Sina Tebianian, John Grace, Jamal Chaouki, Thomas Leadbeater, Rouzbeh Jafari, David Parker, et al.

Development and confirmation of a simple procedure to measure solids distribution in fluidized beds using tracer particles

Yupeng Xu[1,8], Tingwen Li[2], Liqiang Lu[1,9], Xi Gao[1,8], Sina Tebianian[3], John R. Grace[6], Jamal Chaouki[4], Thomas W. Leadbeater[7], Rouzbeh Jafari[4], David J. Parker[5], Jonathan Seville[5], Naoko Ellis[6]

[1] National Energy Technology Laboratory, U.S. Department of Energy, Morgantown, WV, USA
[2] SABIC Corporate Research and Development, Sugar Land, TX, USA
[3] IFP Energies Nouvelles, Process Design and Modeling division, Lyon, France
[4] Département de génie chimique, Ecole Polytechnique, Montréal, QC Canada H3T 1J4.
[5] Positron Imaging Centre, University of Birmingham, Birmingham, B15 2TT, UK
[6] Department of Chemical & Biological Engineering, University of British Columbia, Vancouver, Canada V6T1Z3
[7] Department of Physics, University of Cape Town, South Africa
[8] Leidos, Inc., Reston, VA, USA
[9] West Virginia University Research Corporation, Morgantown, WV 26506, USA

* Corresponding author: litingwen@gmail.com

Abstract
The spatial distribution of solid particles is a key factor affecting the performance of fluidized bed reactors. Non-invasive techniques including radioactive particle tracking (RPT) and positron emission particle tracking (PEPT) are deployed to measure the solids distribution. Different methods to calibrate the particle tracking measurements have been developed to quantify mean solids concentration. In this paper, gas-solid flows in a traveling fluidized bed are simulated with CFD-DEM and the behavior of different particles, including bulk sand particles and tracer particles are investigated. The simulated hydrodynamics are compared with experimental measurements. Analyses are carried out to derive the mean solids concentration from the tracer particle data. Different calibration approaches are examined, and the simple calibration method is verified. It is shown that the mean solids concentration can be measured reliably using representative tracer particles. The experimental RPT data are then revisited with the new calibration method which yields more realistic results.

Key words: coarse grained method; travelling fluidized bed; tracer particles; solids volume fraction; particle tracking, computational fluid dynamics

Highlights:
Travelling fluidized bed is simulated with a coarse-grain CFD-DEM
The solids distribution derived from tracer data is verified numerically
A simple calibration method is examined and shown to be effective
Experimental data are revisited with the new calibration method

1. Introduction

Gas-solid fluidized beds are widely used in energy and chemical industry applications due to their good mixing and heat transfer ability. However, design and scale-up of fluidized bed reactors and optimization of the reactor performance are hindered by the lack of fundamental knowledge of physical phenomena occurring in these systems. In different offices and labs around the world, gas-solid fluidized bed reactors are being designed, experimentally tested and investigated. Various invasive and non-invasive experimental techniques have been

developed for hydrodynamic study of fluidized beds, but the merits and reliability of each measurement technique have not been challenged under a unified framework. In recent years, an effort to benchmark different experimental techniques in a small-scale fluidized bed system called a "traveling fluidized bed" led by the University of British Columbia has been reported (Dubrawski et al., 2013; Tebianian et al. 2016a). This traveling fluidized bed is an experimental setup of simple and elegant design which has been shipped to laboratories in three countries together with two types of particulate materials to conduct experimental measurements at the same operating conditions in order to benchmark different measurement techniques. Overall, the key hydrodynamic measurements, including local solids concentration (or voidage), particle velocity and solids flux, determined by different experimental techniques produced reasonable qualitative agreement, but significant quantitative discrepancies (Tebianian et al., 2015, 2016a, 2016b).

With the development of innovative numerical schemes and advanced computer hardware, CFD numerical simulation is becoming more and more reliable, capable not only in comparison with small lab-scale experimental setup, but also in predicting relatively large scale full-loop fluidized bed systems. To this end, the experimental data collected through different techniques from the traveling fluidized bed provide valuable data for testing the validity of numerical simulations, with good indication of experimental error. Several comparisons have been reported in the literature on numerical simulation of the traveling fluidized bed. Gao (Gao et al., 2018a, 2018b) assessed the mesoscale solid stress in coarse-grid TFM simulation and an enhanced filtered drag model by comparing numerical results with experimental measurements. Vashisth et al. (2015) compared predictions of the EMMS drag model against experimental data from the traveling fluidized bed. In each of these cases, experimental data obtained by different measurement techniques provided a benchmark database for evaluation of CFD models.

Numerical simulations have also been used to help understand discrepancies among different experimental measurements and to gain insight into fluidized bed behavior. Xu et al. (2019a) conducted CFD-DEM simulations of the traveling fluidized bed by tracking different tracer particles to study the particle velocity inside the system. Their results showed that the RPT and PEPT tracer particles used under identical experimental conditions were capable of measuring bulk flow velocities, and discrepancies between results obtained by two different tracer methods were not caused by the differences in the size or density of the tracer particles. They further compared two methods used to determine averaged velocities through particle tracking techniques, i.e. face-average approach – averaging velocities of particles crossing a virtual plane over a period of time, and volume-average approach – averaging velocities of particles passing through a defined volume over time. Their study showed significant differences between both computational and experimental results based on these two approaches.

Among different hydrodynamic variables measured in the traveling fluidized bed system, the solid holdup (or voidage) is the most fundamental one. It has been measured with Electrical Capacitance Tomography (ECT), X-ray Computed Tomography (XCT), Radioactive Particle Tracking (RPT), as well as spatially averaged values derived from pressure gradients and bed expansion. For the range of experimental systems and operating conditions studied, it was found that local average solid holdup measured based on different experimental techniques varied from 0.20 to 0.45 at different locations within the bed (Dubrawski et al., 2013).

In this study, we first verify the applicability of predicting typical square-nose slugging phenomena in the travelling fluidized bed using coarse-grain CFD-DEM simulation. Then, we describe the detailed methodology for obtaining the bulk solids volume fraction through tracer particles, together with different calibration methods. A simple calibration method is verified numerically with respect to axial and radial solid distributions. The calibration method verified in the current study is then applied to the RPT and PEPT experimental data for comparison with other measurements and previous analysis using a complicated calibration procedure.

2. Coarse-grain DEM

Numerical simulation is a powerful tool for modeling gas–solid motion. Various models have been used to predict the performance of fluidized systems of different scales (Lu et al., 2018; Xu et al., 2017a, Verma et al. 2016). Among those models, CFD-DEM, where particle motion, collisional forces and gas-particle interactions are included, has been demonstrated to be able to capture key flow features such as bubbles and clusters. Also, particle-scale information, including residence time, collisional forces, and dispersion intensities, are available for detailed analyses of complex flow phenomena. However, computational expense is high, historically limiting the application of CFD-DEM to small-scale systems (Li et al., 2017; Xu et al., 2017b). Today, even with the advanced parallelization technique and latest hardware, simulations are typically limited to a maximum of tens of million particles (Walther and Sbalzarini, 2009; Jajcecic et al., 2013; Yang et al., 2015; Tsuzuki and Aoki, 2016). It is common that fine particles, usually smaller than 100 μm, are used in industry. A system with 100 particles of 100 μm diameter in each direction, i.e. a 1-cm cube, contains 1,000,000 particles, already expensive for CFD-DEM simulation, while commercial systems deploy billions of particles.

Simulations reported here were conducted using the open source Multiphase Flow with the Interphase eXchanges (MFiX) code. Gas flow is modeled by solving the averaged Navier-Stokes equations for mass and momentum conservation, whereas the solid phase is modeled by tracking individual particles using a discrete element method (DEM). Full details on the governing equations, together with the numerical implementation and coupling procedure, are not presented here, but can be found elsewhere (Garg et al., 2012; Xu et al., 2019b). Basically, the motion of particle is described by Newton's equations of motion, and the coarse-grain technique is used to accelerate the computational speed by lumping many particles into parcels to reduce the particles count (Sakai et al. 2014, Lu et al. 2016).

It is important in the current study to simulate the full particle size distribution (PSD) of the bed material and account for the detailed physical properties of the tracer particles. It is straight-forward to incorporate an arbitrary distribution of particle properties, like size and density, in DEM simulations. In the current research, different statistical weights are assigned to particles of different diameters, while the original poly-disperse powder is scaled to a coarse mono-disperse system with the same parcel size. Lu et al. (2018) compared two types of coarse-grain methods for a poly-disperse system. The second approach, utilized in the current research, was found to be suitable for fully fluidized system and it provided greater computational efficiency than the first approach. By varying the real particles represented by the coarse-grain numerical parcel, the full particle size distribution was captured. The schematic in Fig. 1 illustrates how the coarse-grain approach is used in the current study to accelerate the simulation. Instead of tracking each individual particle, larger coarse-grain parcels are solved to represent groups of true particles having identical properties. Details on

coarse-grain CFD-DEM and its verification, validity and uncertainty, as well as its application on multiscale problem can be found elsewhere (Lu et al., 2016). The applicability of this method in modeling the traveling fluidized bed, has been tested in the previous work which compared different tracer particles and averaging techniques for particle velocities in a fluidized bed with experimental results (Xu et al., 2019).

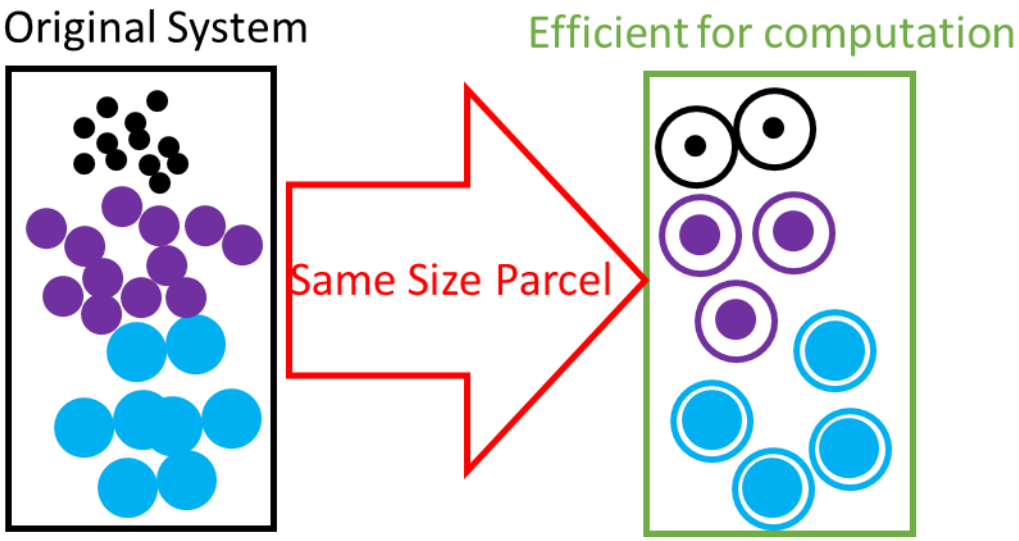

Fig. 1. **Coarse-grain strategy for a polydisperse system.**

3. Simulation setting

The travelling fluidized bed is a robust and versatile test platform for benchmarking different experimental instrumentations (Dubrawski et al., 2013). The fluidized bed column and its auxiliary apparatus can be easily disassembled, transported and remounted, ensuring identical operation in different locations. The main component is a vertical cylindrical fluidization column consisting of a 0.96 m long × 0.133 m i.d. dense bed section, surmounted by a 1.36 m long × 0.190 m i.d. freeboard section, with an inclined transition at 30˚ to the vertical. This configuration is illustrated in Figs. 2(a) and (b).

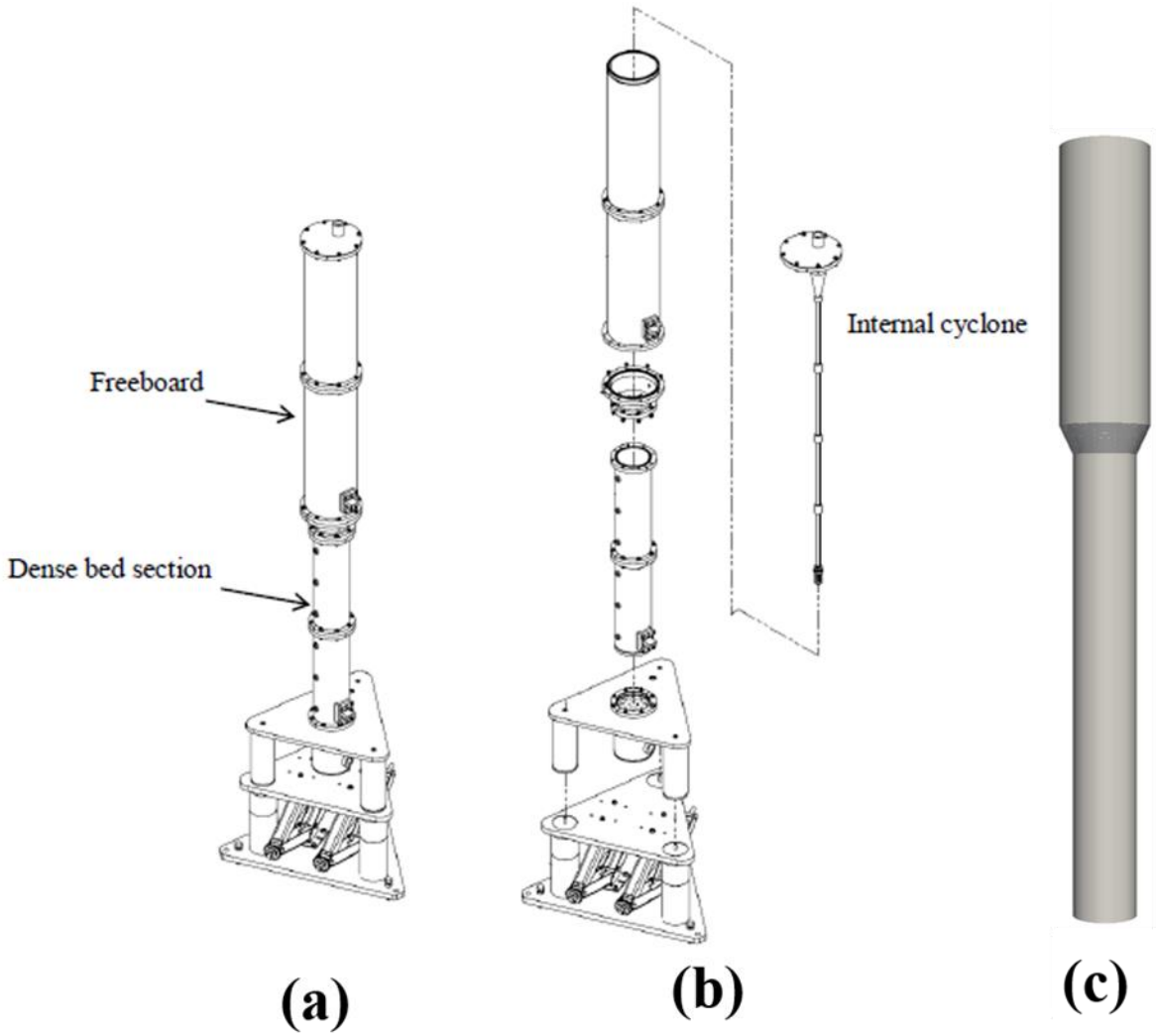

Fig. 2 Traveling fluidized bed (TFB) column: (a) assembled experimental setup; (b) disassembled view; and (c) simulation geometry.

Silica sand (Lane Mountain LM50) particles were used as the fluidized material. These particles travelled together with the equipment to further ensure identical operating conditions at each participating location. The Sauter mean diameter (d_{32}) of the sand particles is about 302 µm, and the particle density is 2644 kg/m^3, with a minimum fluidization velocity of 0.0796 m/s and a terminal settling velocity in air of 0.73 m/s. The powder belongs to Geldart group B. The particle size distribution used in the simulation, which is the same as the experimentally measured particle size distribution, is plotted in Fig. 3. Experiments were conducted using the RPT and PEPT techniques to measure the solid velocity of the bulk bed material inside the system. For each measurement, a single tracer particle with density and size as similar as possible to the bulk particles, was tracked as it travelled in the system for an extended time period. The key properties of the bulk material and tracer particles are provided in Table 1.

Table 1: Key properties of bulk sand particles and tracer particles used in the experimental study

Particles:	**Sand**	**RPT tracer**	**PEPT tracer**
Density (kg/m^3)	2644	2000	3000
Diameter (mm)	0.312 to 0.292	0.400 (single	0.300 (single

	(Sauter mean)	particle)	particle)
Shape	Irregular	Nearly spherical	Irregular
Number of Particles	3,034,944	1000	1000

In current simulations, the computational domain is confined to the bed section and the disengagement zone as shown in Fig. 2(c). The density (ρ_g) and viscosity (μ_g) of the fluidizing gas (air) are set to 1.205 kg/m^3 and 1.8 × 10^{-5} Pa.s, respectively. Air flows into the bed from the bottom, with a constant gas inlet velocity boundary condition, and leaves from the top, with a constant gas outlet pressure boundary condition. A no-slip wall boundary condition is used for the gas phase. The MFIX Cartesian grid cut-cell technique is used to specify the geometry, in which a Cartesian grid is used to discretize the computational domain, while boundary cells are truncated to resolve the shape. Details on the Cartesian grid cut-cell method are available elsewhere (Dietiker, 2015; Kirkpatrick et al., 2003).

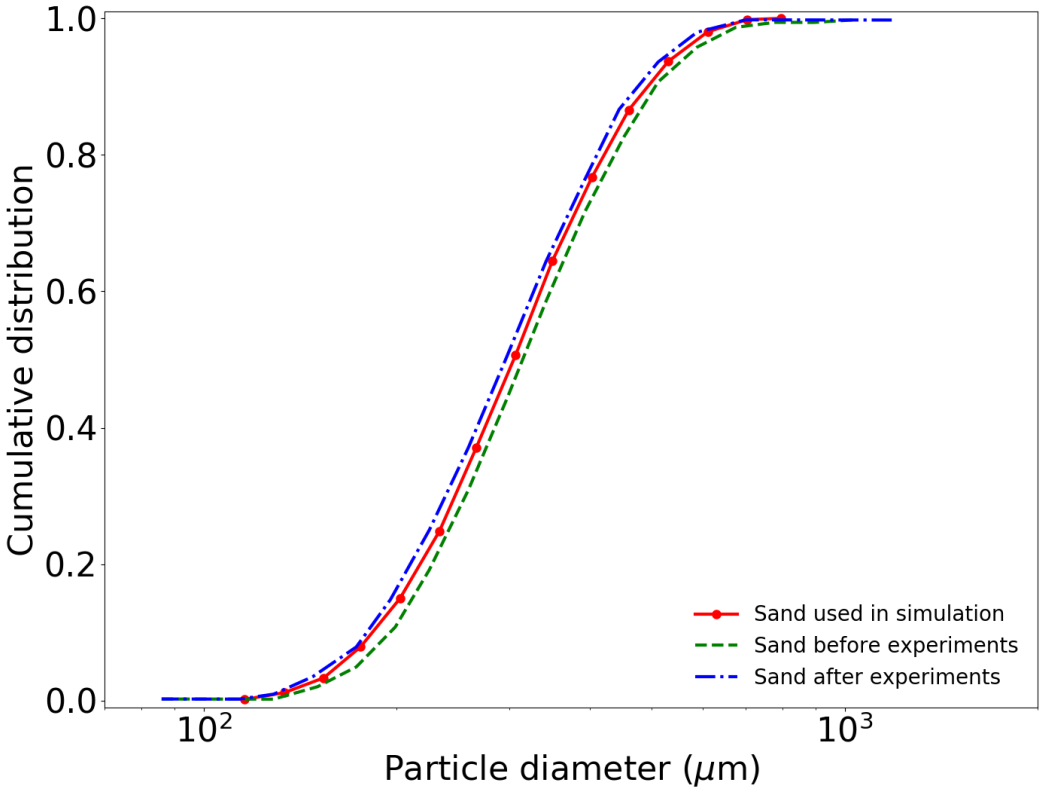

Fig. 3 Particle size distribution of sand used in the experimental tests.

In the simulations, each numerical parcel is of identical size, d_p = 1510 μm, representing many real particles. By varying the number of real particles represented by a numerical parcel, particles of different sizes can be simulated with the same parcel size. In total, about 3 million numerical particles with their key physical properties corresponding to the silica sands were tracked, with the cumulative particle size distributions (PSD) shown in Fig. 3. The particles size, before and after the experiments, was determined by a Malvern Instruments MasterSizer 2000. As can be seen from Fig.3, the sand particles became slightly finer after the experimental run, presumably due to attrition. Without accounting for this size change, a mean distribution was used in the simulation. Different tracer particles with a specific size

and density were simulated including 1000 RPT particles, 1000 PEPT particles and 1000 sand tracer particles. The bed was fluidized, reaching a stable state within a few seconds, with 110 s of simulation conducted in total. In post-processing, the first 10 s were discarded to exclude start-up effects. During the simulations, tracer locations and velocities were saved at 100 Hz, whereas the Eulerian grid-based flow field was saved at 20 Hz for verification of flow field information derived from the tracer data.

4. Results and discussion

4.1 Predicting square-nosed slug flow in travelling fluidized bed

In the TFB experiments, the bed of sand particles was operated in the square-nosed slugging flow regime (Tebianian et al., 2016a), instead of the more common axial-symmetric round-nosed slug flow regime in which bullet-shaped slugs rise through the dense phase which flow downwards in an annular region surrounding the slug, close to the wall. According to Grace (1982), square-nosed slugging mainly happens in columns with smooth wall, with the slugs then occupying the entire cross-section of the column. The upward movement of the interfaces is slow, and largely caused by particles raining down from the roof of the slugs through the dilute gas slugs to their floors.

In the current work, two superficial velocities, 0.4 and 0.6 m/, were simulated. The results showed that the square-nosed slugging flow regime can be captured successfully with a combination of particle-particle (0.6) and particle-wall (0.1) friction coefficients, as shown in Fig. 4. The formation of a squared-nosed slug, its movement and burst at the top of the bed are shown. Small bubbles formed right above the distributor plate grow through coalescence and finally occupy the whole column cross-section to form the square-nosed slugs. The square slug rises slowly as particles rain downward from the underside of the roof. Fingering due to Rayleigh-Taylor instability can also be observed. Occasionally, a square-nosed slug transforms into round-nose slug causing solids to move downward along the wall.

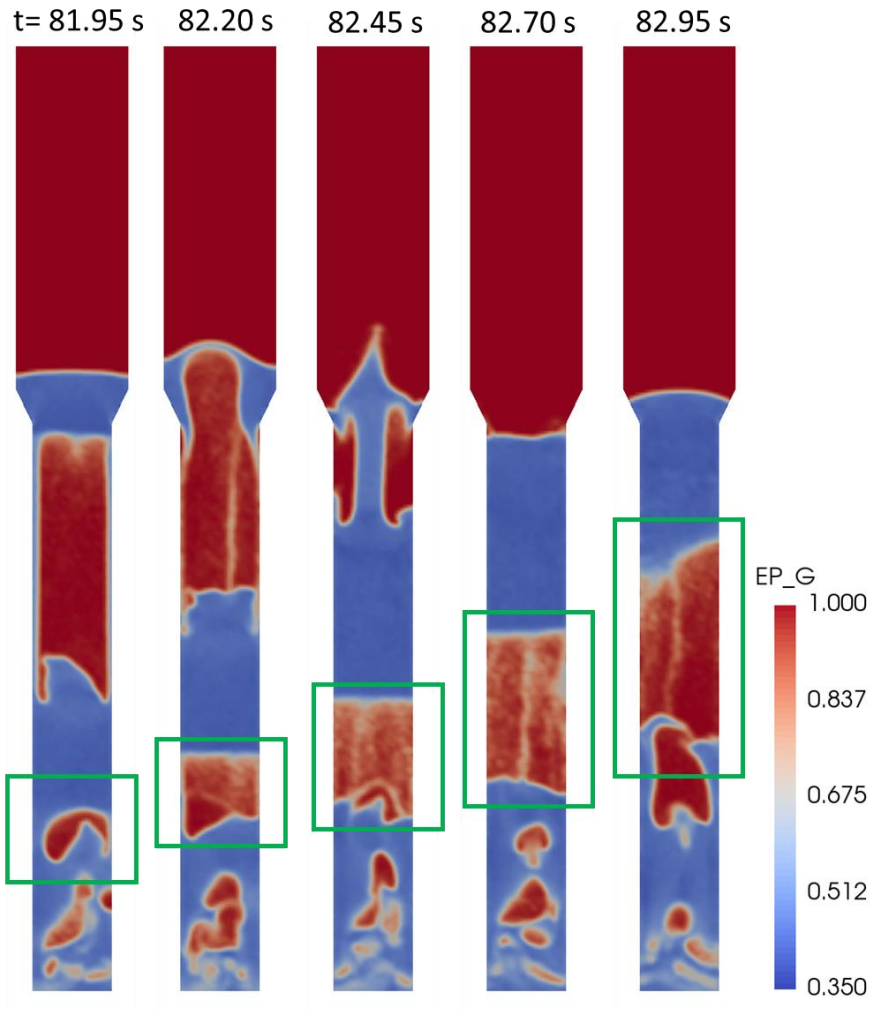

Fig 4. Simulation results showing formation, movement and burst of a typical square-nosed slug for a superficial gas velocity of 0.4 m/s

Transient results for the gas volume fraction, vertical component of gas velocity, vertical component of solids velocity and the particle size distribution along the axial direction are shown in Fig 5. Note that all quantities presented in Fig. 5 are calculated based on the fluid cells. For example, the mean solid velocity and Sauter mean diameter of particles are calculated in each fluid cell by averaging over all particles in that cell.

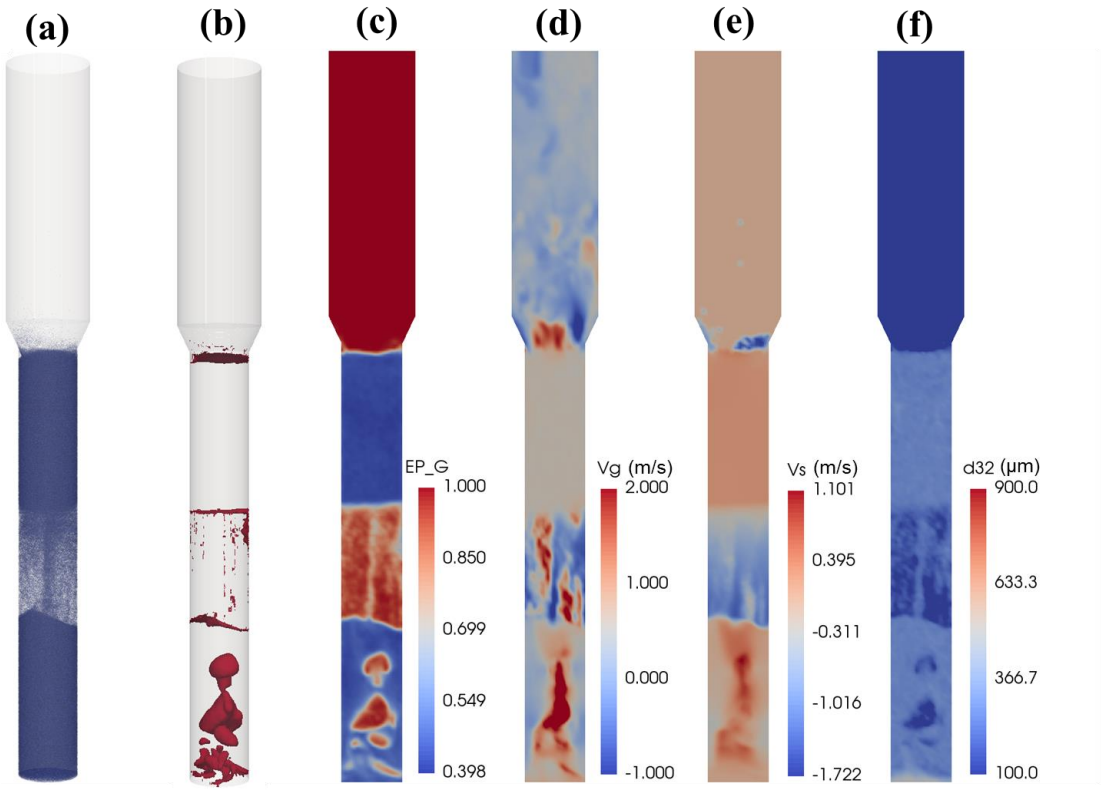

Fig. 5 Transient simulation results at t=82.70 s: (a) Particle distribution along the bed; (b) contour plot of voidage of 0.65; (c) local voidage; (d) vertical component of gas velocity (m/s); (e) vertical component of solid velocity (m/s); and (f) mean particle diameter (μm) (V_s: solid-phase vertical component of velocity calculated by averaging particle velocities in each fluid cell; d_{32}: Sauter mean diameter of particles in each fluid cell. (U_g=0.40 m/s).

Time-average results for the gas volume fraction, vertical component of gas velocity, vertical component of particle velocity and time-average distribution of mean particle diameter are shown in Fig 6. Overall, the flow is relatively dilute in the central region and dense near the wall. Transition from the bubbling flow regime in the lower region to the slugging regime in the upper region can be identified. The numerical simulations provide predictions that are qualitatively consistent with the experimental observations.

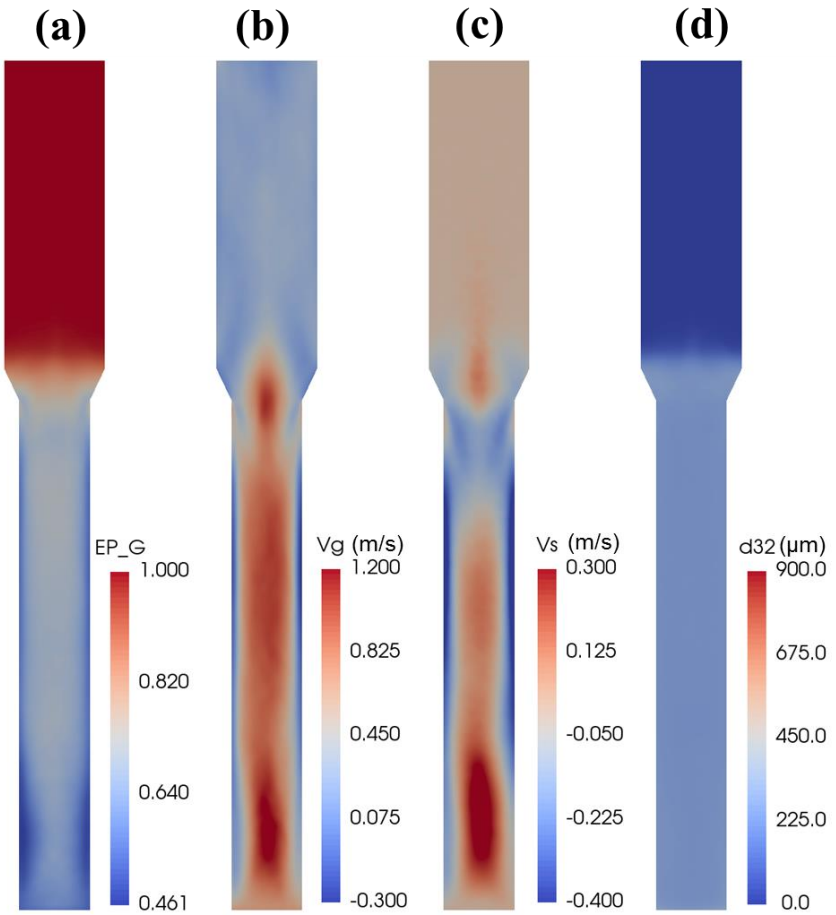

Figure 6. Sliced view of time-average results for a superficial gas velocity of 0.4 m/s: (a) time-average gas volume fraction; (b) time-average vertical component of gas velocity (m/s); (c) time-average vertical component of particle velocity (m/s); and (d) time-average distribution of mean particle diameter.

4.2 Estimation of the solids volume fraction with tracer particles

Two tracer techniques - RPT from the Ecole Polytechnique de Montréal and PEPT from the University of Birmingham - were used to measure particle velocities in the traveling fluidized bed. The data were further analyzed to determine the solids spatial distribution. These two methods are non-intrusive, which should contribute to measurement accuracy. In this section, experimental procedures for measuring the solids spatial distribution are utilized in the CFD-DEM simulation to verify the methodology.

In the experiments, one tracer particle was followed, with its position and velocity recorded at finite time intervals. By collecting such data for long enough times, the mean solid concentration can be deduced from the averaged possibility in the control volume of interest. In practice, it is very difficult to conduct simulations lasting hours, even for many minutes, especially with millions of particles in the Euler-Lagrangian method. Therefore, in the current simulations, instead of simulating an individual tracer particle, 1000 of each of three different types of tracer particles, were tracked for 100 s. Xu et al. (2019) showed that with this method, the average bulk particle velocities can be obtained successfully through the information obtained from tracer particles.

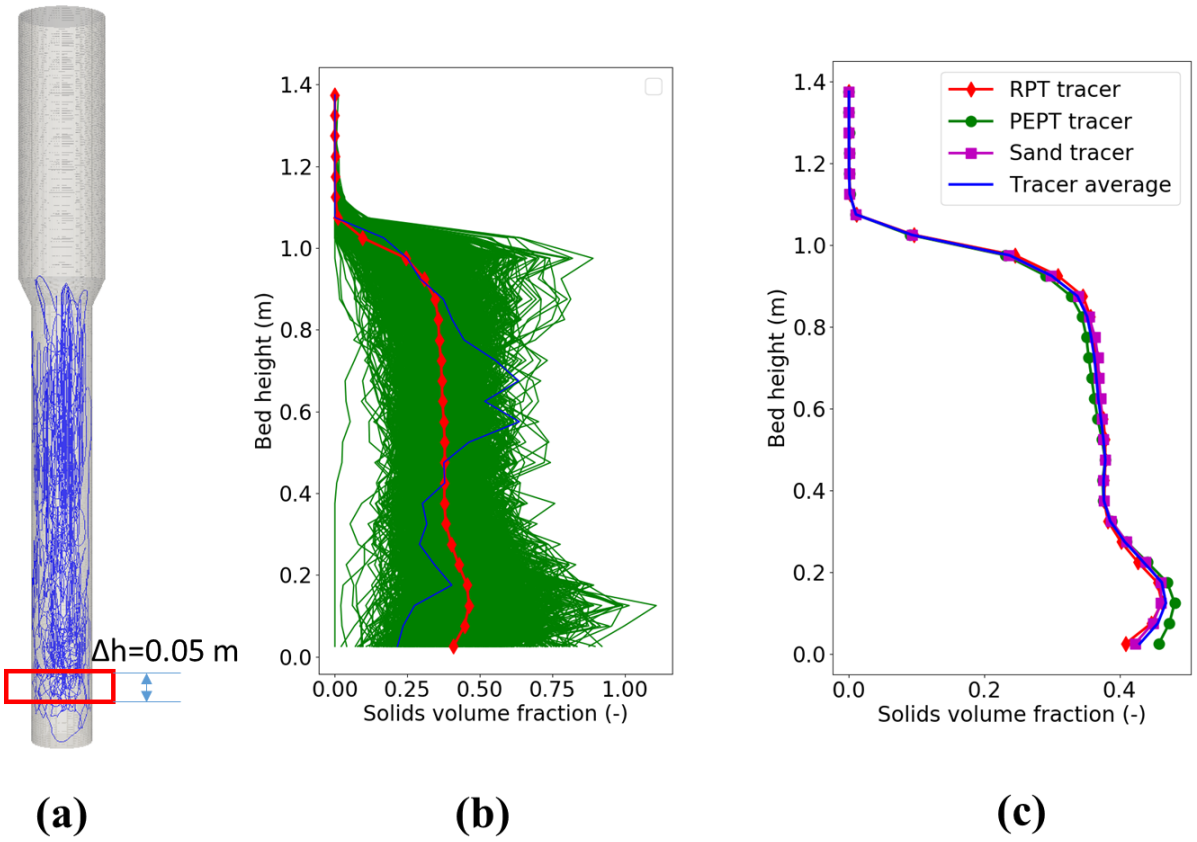

Fig. 7(a) Trajectory of 1 of 1000 simulated RPT tracer particles for a superficial gas velocity of 0.4 m/s; (b) Cross-section averaged solids volume fraction from one RPT tracer particle (blue line), the other 999 RPT tracer particles (green line) and the average solids volume fraction of the 1000 RPT tracer particles (red line); (c) Average solids volume fraction profiles of three different types of tracer particle and corresponding average profiles.

The solids volume fraction of the bulk particles in the control volume can be obtained from the tracer particle information. The voidage in each control volume can be determined by the number of counts with RPT method or determined by the pseudo-density maps or "occupancy" with the PEPT method (Seville et al., 2009; Stein et al., 1997). However, it is vital that these methods be calibrated properly. The processing required several steps. Here we use the solids volume fraction along the axial direction as an example: First, by tracking the movement of each tracer particle at a frequency of 100 Hz, the trajectory of each tracer particle can be obtained. In Fig. 7(a), the trajectory of 1 of 1000 simulated RPT tracer particles for a superficial gas velocity of 0.4 m/s is shown by blue lines for the entire simulation of 100 s. The bed was divided into sections along the axial direction with Δh=0.05 m for each, as shown in Figure 7(a). Then the appearance of this tracer particle in each section was counted, and then divided by the total number recorded, as detailed below. Next, the trajectories of all the other 999 RPT particles were treated in the same manner, as shown by the green lines in Fig. 7(b), and average values were obtained by averaging the 1000 RPT particles, as shown by the red line in Figure 7(b). Finally, all three tracer particles were analyzed as shown in Fig. 7(c), which indicates that the three tracer particles provided very similar results. The average solids volume fraction along the axial direction can then be obtained by averaging the three data sets corresponding to the different tracer particles.

A much simpler calibration method was used in this research. We count the number of appearances (x_i) of each tracer particle in a volume (v_i) of interest in the time span, then

divide by the total number of appearances (X) registered in the whole bed. When particle tracking in the whole bed is not available, for example for the PEPT measurements, the total number of appearances can be simply estimated from tracking duration and frequency. The possibility (y) of a particle on average being located in the volume of interest in the time span is then

$$y_i = \frac{x_i}{X} \tag{1}$$

Since there are n_p particles in the bed, the solids volume fraction can be calculated as

$$\varepsilon_{si} = \frac{y_i n_p v_p}{v_i} \tag{2}$$

where v_p is the volume of each particle.

Experimentally, two different methods were reported by Dubrawski et al. (2013). One involved dividing the number of counts registered in a particular (x,y,z) cell by the total number of counts registered. Then divide by the fractional volume occupied by the cell, and multiply by the bulk solids volume fraction of the particle. This method can be expressed as:

$$\varepsilon_{si} = \frac{y_i}{\frac{v_i}{V_{\text{Total}}}} \times \frac{n_p v_p}{V_{\text{Total}}} = \frac{y_i n_p v_p}{v_i} \tag{3}$$

where V_{Total} is the average volume occupied by the particles, which can be determined knowing the average bed height. Ultimately, this method is similar to the approach used in the simulation if the V_{Total} is cancelled out, as shown in Equation (3).

Another method was to divide individual cell counts by the number of counts of the slowest detectable tracer velocity, and assume that the corresponding slowest particle is moving at the minimum fluidization velocity. The solid volume fraction in each cell can then be obtained by calibrating against the solid volume fraction at minimum fluidization. However, it is impossible to confirm that the slowest tracer velocity corresponds to the minimum fluidization state.

For the tracer particles used, the influences of the tracer particle number and the average time span need to be studied. Considering the variation in profiles shown in Fig. 7(b) by different tracer particles, many data are needed to obtain statistically converged results. The average solids volume fractions obtained from different numbers of tracer particles and different time durations are shown in Fig. 8(a). The estimated solid volume fractions are quite robust and show relatively weak dependence on the tracer count and sampling period. As can be seen, when there are more than 500 tracer particles with an average time of 100 s, no noticeable difference can be seen. The results hereafter are from 1000 tracer particles with an average time span of 100 s.

On the other hand, with the CFD simulations, the average solids volume fraction along the axial direction can be obtained directly. Then the solids volume fraction obtained from the tracer particles can be compared against the true quantity calculated directly in the CFD simulation. The results are shown in Fig. 8(b). Clearly, a good match was found along the bed. It should be noted that the method requires the tracer particle to be representative of the bulk

solids. This is usually achieved by carefully choosing the physical properties for the tracer particle. However, the accuracy will be compromised when significant size/density distributions exist and segregation takes place. In addition, the method tends to fail if there is a stagnant zone with limited solid mixing, preventing the tracer from passing through.

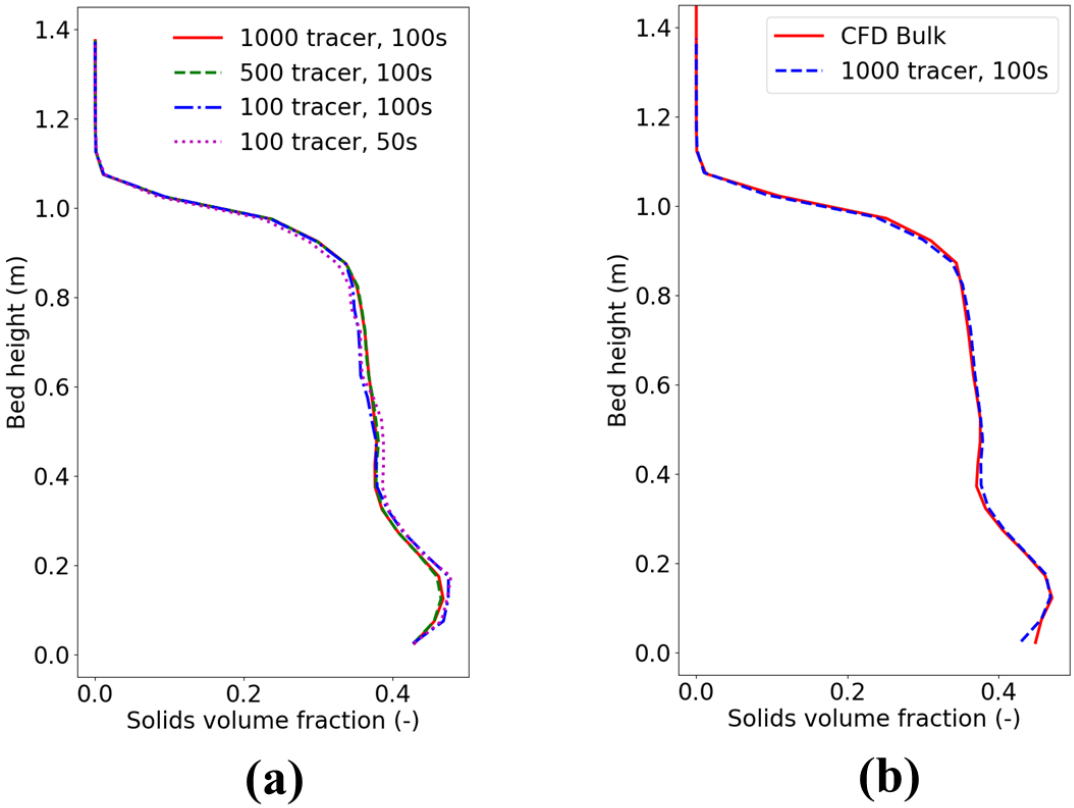

Fig. 8 (a) Average solids volume fraction obtained from different numbers of tracer particles followed for different durations; (b) Comparison of solids volume fraction from the tracer particles and values predicted by CFD.

4.3 Comparison of model predictions and experimental measurements

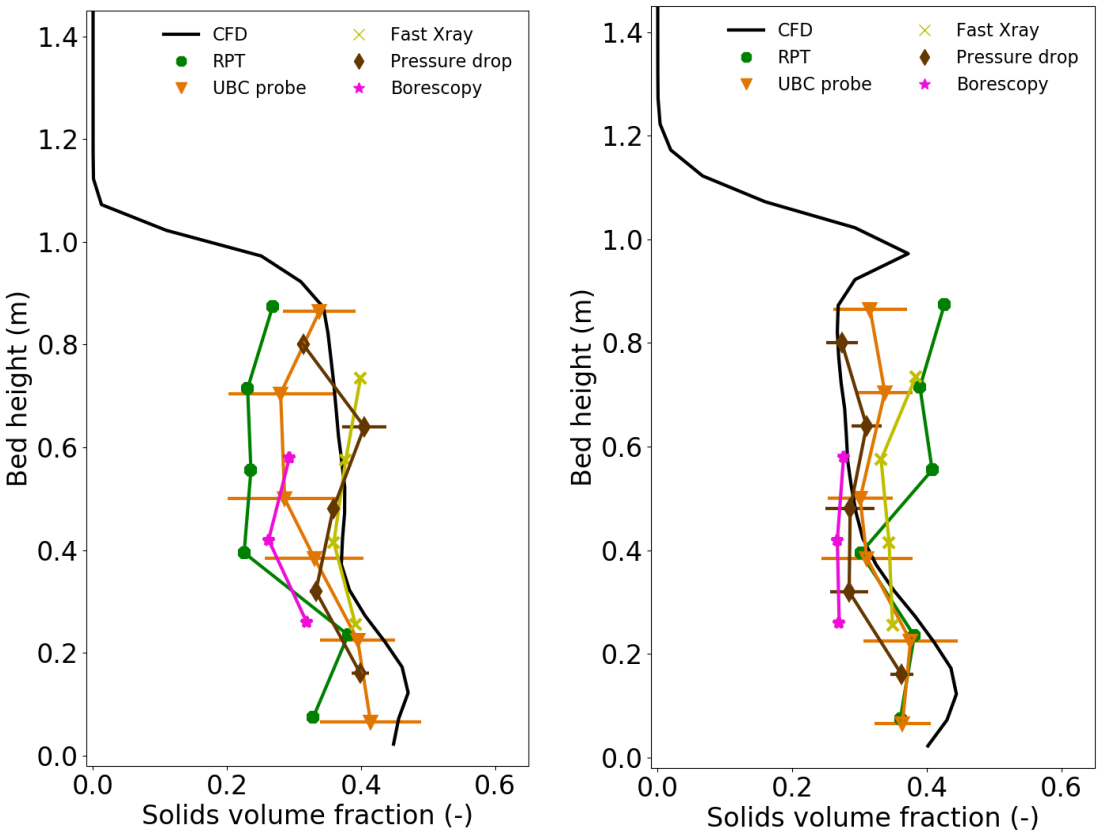

Fig. 9. Comparison of cross-sectional average solids volume fraction along bed provided by simulation and different experimental techniques: (a) U_g=0.40 m/s; (b) U_g=0.60 m/s.

Further comparisons of the simulation and experimental results from five different experimental techniques, including both invasive and non-invasive techniques, are shown in Fig. 9. Since there was little difference between direct CFD prediction and estimation from different tracer particles, only the former is shown in the comparison for simplicity. Fig. 9 indicates that for both superficial gas velocities, U_g=0.40 and 0.60 m/s, the numerical results are in reasonable agreement with the experimental data. However, there are considerable discrepancies among the experimental data obtained based on different analysis techniques, with the experimental RPT data showing the greatest deviation from the other experimental measurements. For the RPT data, the calibration approach was based on the minimum fluidization state (Dubrawski et al., 2013) which is believed to be inaccurate. It is difficult to comment on the cause of the discrepancies of the other techniques. However, it is notable that the simulation results match well with the data from pressure drop measurement, the standard experimental method for measuring the axial solids holdup.

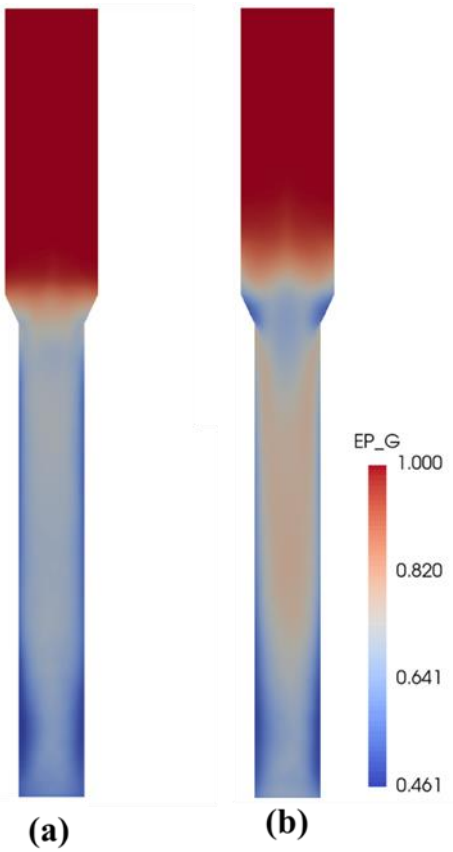

Fig. 10. Sliced view of time-average gas volume fraction for superficial gas velocities of: (a) 0.4 m/s; and (b) 0.6 m/s

4.4 Comparison of radial average voidage profiles

Tracer particle data can also be used to estimate the radial solids volume fraction, following the same process as in the previous section with the same calibration procedure. Here the solids volume fraction is averaged over concentric rings with a spacing of 10 mm in the radial direction and 30 mm in the vertical direction. Axial flow symmetry is assumed for both cases. As can be seen in Fig 11 for U_g=0.40 m/s at a bed height of 0.24 m as an example, three sets of tracer particles predict very similar radial profiles of solid volume fraction. In addition, the average profiles for all three different tracer particles match well the profile obtained directly from the simulation. The sensitivities of the radial profile with respect to the number of tracer particles and duration of sampling are illustrated in Fig. 11.

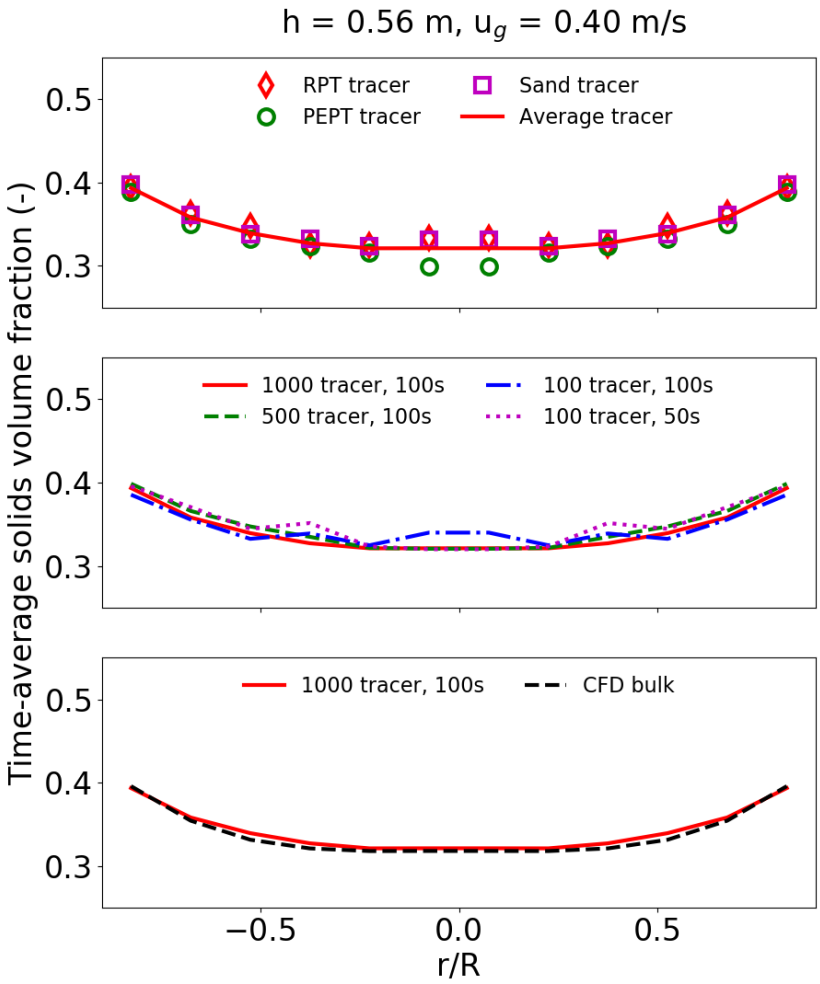

Fig. 11. Radial profiles of time-averaged solids volume fraction from three different tracer particles compared with bulk profile predicted by CFD simulation: (a) Average radial solids volume fraction profiles of three different types of tracer particles and their average profiles, (b) Average radial solids volume fraction obtained from different numbers of tracer particles and different durations; and (c) Comparison of radial solids volume fraction from the experimental tracer particles and values predicted by CFD.

Further comparison of radial profiles of solid volume fraction with experimental data is shown in Fig. 12 for a gas velocity of 0.40 m/s at different heights. Again, there is reasonable agreement between numerical predictions and experimental measurements. However, the experimental RPT measurements deviate significantly from the data derived by other techniques and numerical simulation. Close examination of the experimental technique and its calibration procedure may be helpful to understand the cause of this discrepancy.

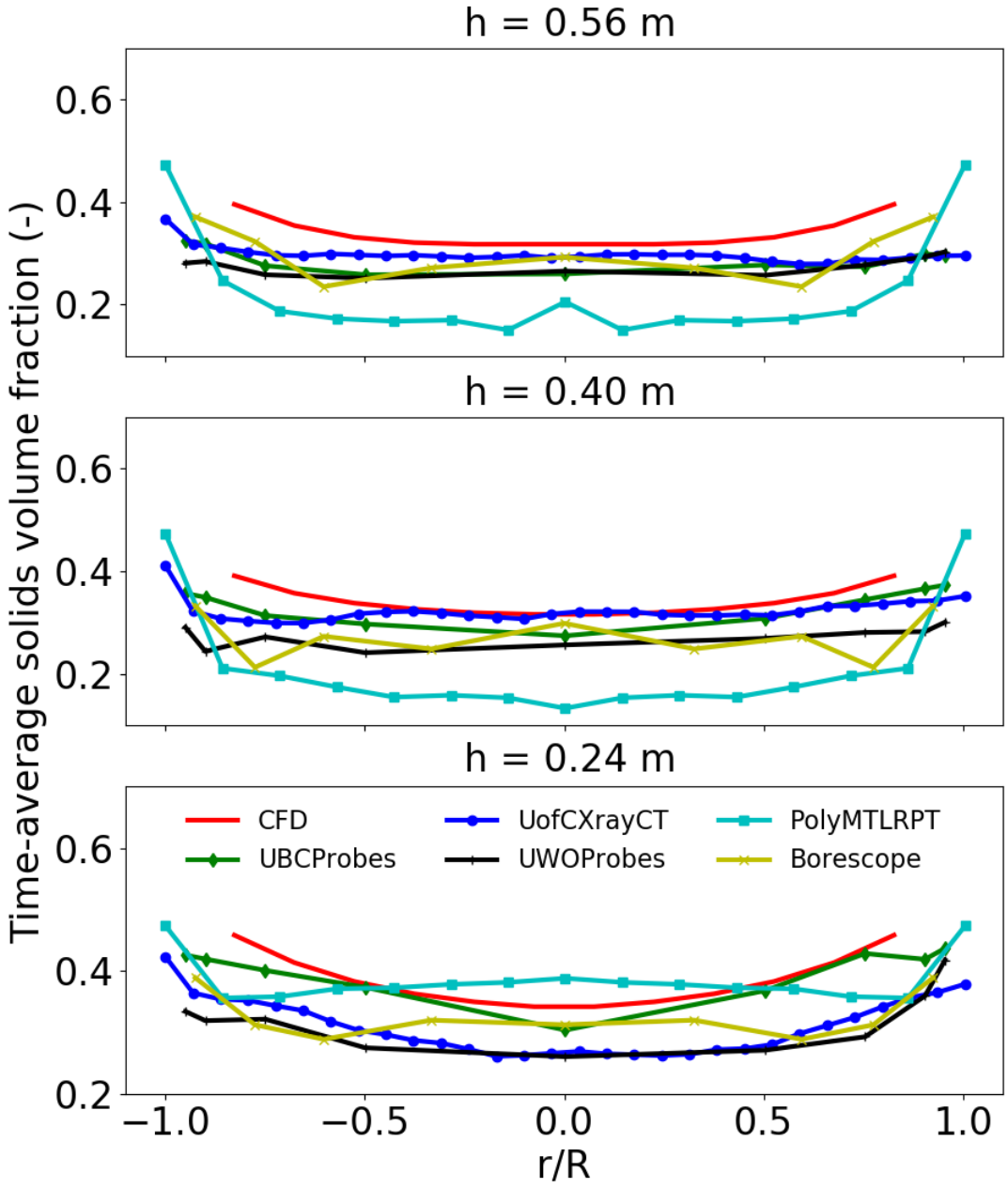

Fig. 12. Comparison of radial solids volume fraction at three heights obtained by tracer particle experimental measurements and CFD bulk simulations for U_g=0.40 m/s.

4.5 Revisitation of RPT experimental data

For the RPT results included in the previous comparison, the method used to calibrate the measurements and to obtain solid concentrations was based on the assumed slowest detectable tracer velocity in the measurement (Dubrawski et al., 2013). However, it is not straightforward to link that to the state of minimum fluidization. On the other hand, it is of interest to see how the simple calibration method performs when applied to the experimental

RPT data. The raw RPT data which are the locations of tracer particle recorded at 100 Hz for up to 8 hours were reprocessed and the results are compared to the previous data from Dubrawski et al. (2013).

Fig. 13 shows the axial profiles of solid holdup for superficial gas velocities of 0.40 and 0.60 m/s using different calibration methods. The newly processed data show trends that differ from the results reported by Dubrawski et al. (2013). For the higher superficial gas velocity of 0.60 m/s, the new results show greater overall bed expansion and lower solid holdup than for the case with a superficial gas velocity of 0.40 m/s, which is expected from most experimental observations. The old data indicate a much denser bed for U = 0.60 m/s than for U = 0.40 m/s, which is counter-intuitive and inconsistent with the measurements from the other experimental techniques. The simple calibration step described in the current study yields results which are more consistent with the other experimental techniques. The PEPT data are analyzed in the similar manner as shown in Fig 13; note that only the lower section of the bed was examined experimentally. The newly analyzed RPT and PEPT results show improved consistency comparing to the previous RPT results reported in Dubrawski et al. (2013). However, considerable discrepancy still exists above the distributor, needing further investigation.

The effect of sampling time span is examined for the experimental RPT data in Figure 14, with data from different time durations of 0.5, 1, 2, 4 h used to obtain the axial profiles of solids holdup. Compared to the numerical simulation results shown in Fig. 8, the experimental data show stronger dependence on the number of data points, i.e. on the sampling time, than the current numerical results. Similar behavior is observed for the PEPT data. This is attributed to the difficulty in achieving statistical convergence for a single tracer particle compared with thousands of tracer particles which provide much better spatial coverage. Hence, it is important to ensure convergence of experimental data for the target measurements.

Similar analysis can be conducted for the RPT experimental data to obtain the radial profiles of solid concentration at different heights. However, due to the limited number of experimental data points in the small control volume used to extract the radial profile, we conclude that the data were unable to provide statistically converged results in the radial distribution, so that a much longer sampling time is needed.

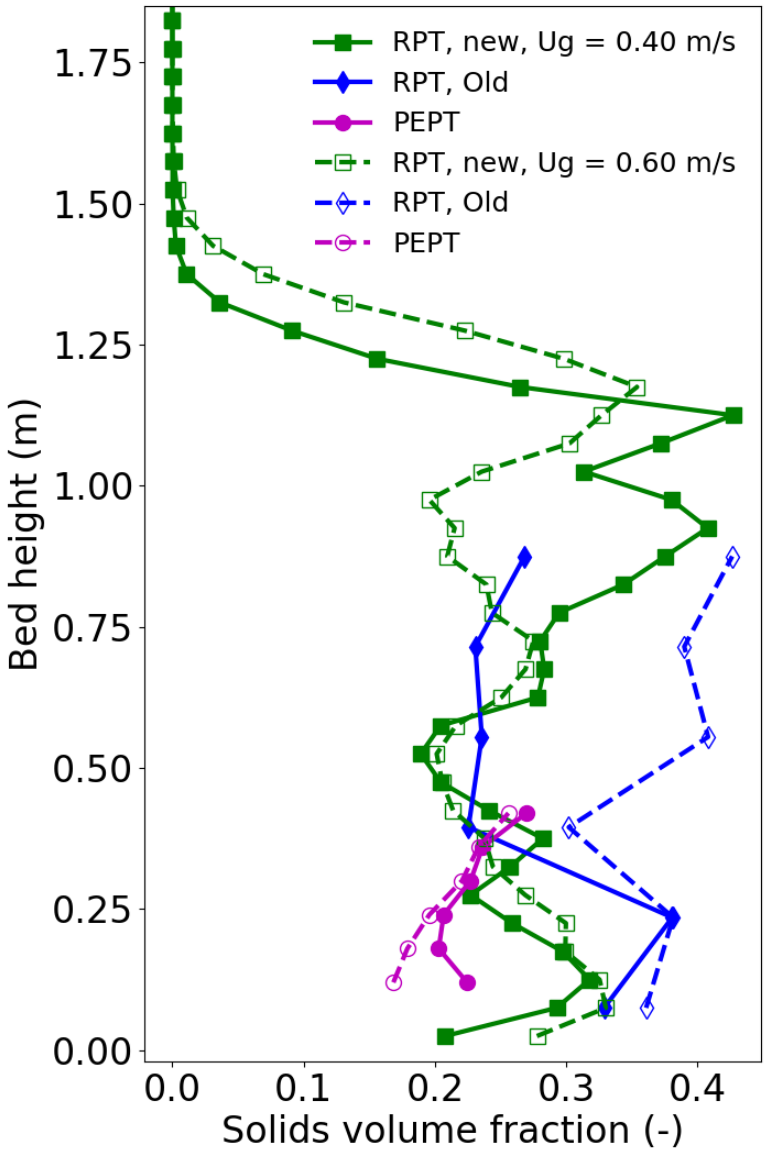

Fig. 13 Vertical profile of cross-sectional average solids volume fraction along bed predicted by RPT and PEPT method calibrated based on this research.

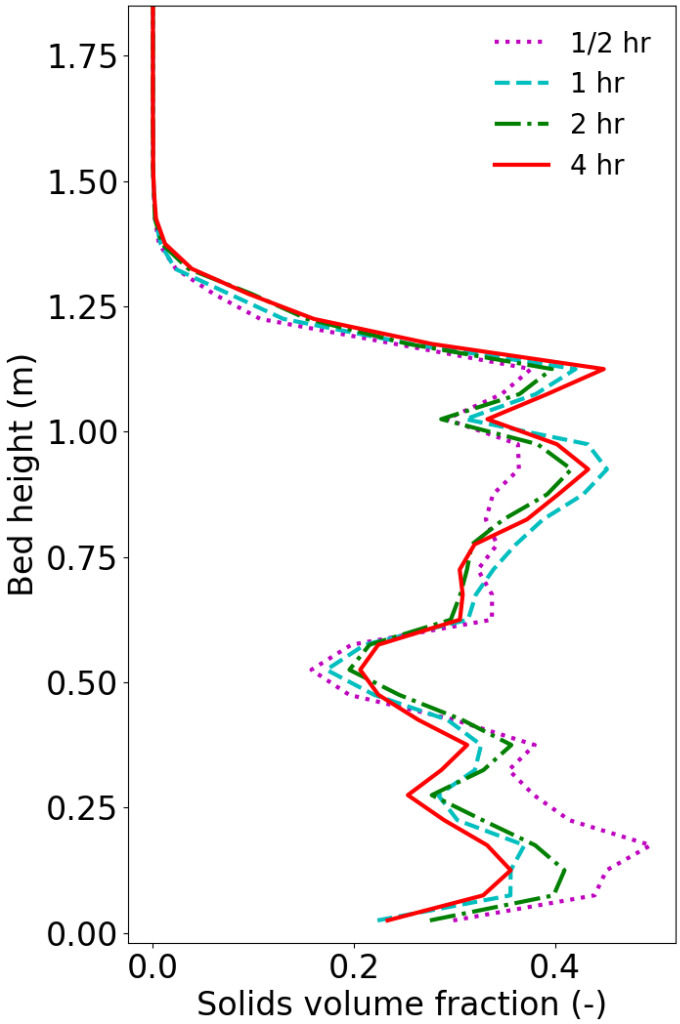

Fig. 14 Effect of sampling time of experimental RPT data on axial profile of solids holdup.

5. Conclusions

CFD-DEM simulations were conducted for the travelling fluidized bed of sand particles. With careful selection of the simulation parameters, especially the particle-particle and particle-wall friction coefficients, experimentally-observed square-nosed slugging behavior was predicted successfully by the simulations. By simulating tracer particles used in the experimental tests, analyses were conducted in the numerical study to extract information on solid volume fraction from tracer data. Three types of tracer particles were considered in the simulation, including RPT, PEPT and sand particles. The mean solid distribution was estimated from the tracer data with a simple calibration method which showed good agreement with the value calculated from the bulk flow. The numerical predictions of solid volume fraction show reasonable agreement with experimental measurements obtained using different techniques, despite the substantial discrepancy among the experimental measurements. When the simple calibration method was further applied to the original RPT experimental data, it yielded more realistic axial profiles of solids holdup.

Acknowledgments

This work was performed in support of the US Department of Energy's Fossil Energy Crosscutting Technology Research Program. The Research was executed through the NETL Research and Innovation Center's Advanced Reaction Systems FWP. Research performed by Leidos Research Support Team staff was conducted under RSS contract 89243318CFE000003.

References

Bellan, S., Kodama, T., Matsubara, K., Gokon, N., Cho, H.S. and Inoue, K., 2019. Thermal performance of a 30 kW fluidized bed reactor for solar gasification: A CFD-DEM study. Chem. Eng. J. 360, 1287-1300.

Dietiker, J.F., 2015. Multiphase Flow with Interphase eXchanges: Cartesian Grid User Guide.

Dubrawski, K., Tebianian, S., Bi, H.T., Chaouki, J., Ellis, N., Gerspacher, R., Jafari, R., Kantzas, A., Lim, C.J., Patience, G.S., Grace, J.R., 2013. Traveling column for comparison of invasive and non-invasive fluidization voidage measurement techniques.

Powder Technol. 235, 203–220.

Gao, X., Li, T., Rogers, W.A., 2018a. Assessment of mesoscale solid stress in coarse-grid TFM simulation of Geldart A particles in all fluidization regimes. AIChE J. 64, 3565–3581.

Gao, X., Li, T., Sarkar, A., Lu, L., Rogers, W.A., 2018b. Development and validation of an enhanced filtered drag model for simulating gas-solid fluidization of Geldart A particles in all flow regimes. Chem. Eng. Sci. 184, 33–51.

Garg, R., Galvin, J., Li, T., Pannala, S., 2012. Open-source MFIX-DEM software for gas–solids flows: Part I—Verification studies. Powder Technol. 220, 122–137.

Grace, J.R., 1982. Fluidized bed hydrodynamics, Section 8.1 in: Handbook of Multiphase Systems, Ed. G. Hetsroni, Hemisphere, Washington.

Kirkpatrick, M.P., Armfield, S.W., Kent, J.H., 2003. A representation of curved boundaries for the solution of the Navier–Stokes equations on a staggered three-dimensional Cartesian grid. J. Comput. Phys. 184, 1–36.

Lu, J., Tan, M.D., Peters, E.A.J.F., Kuipers, J.A.M., 2018. Direct Numerical Simulation of Reactive Fluid–Particle Systems Using an Immersed Boundary Method. Ind. Eng. Chem. Res. acs.iecr.8b03158.

Lu, L., Xu, J., Ge, W., Gao, G., Jiang, Y., Zhao, M., Liu, X., Li, J., 2016. Computer virtual experiment on fluidized beds using a coarse-grained discrete particle method—EMMS-DPM. Chem. Eng. Sci. 155, 314–337.

Lu, L., Xu, Y., Li, T., Benyahia, S., 2018. Assessment of different coarse graining strategies to simulate polydisperse gas-solids flow. Chem. Eng. Sci. 179, 53–63.

Li, T., Rabha, S., Verma, V., Dietiker, J.F., Xu, Y., Lu, L., Rogers, W., Gopalan, B., Breault, G., Tucker, J. and Panday, R., 2017. Experimental study and discrete element method simulation of Geldart Group A particles in a small-scale fluidized bed. Advanced Powder Technol. 28(11), 2961-2973.

Sakai, M., Abe, M., Shigeto, Y., Mizutani, S., Takahashi, H., Viré, A., Percival, J.R., Xiang, J. and Pain, C.C., 2014. Verification and validation of a coarse grain model of the DEM in a bubbling fluidized bed. Chemical Engineering Journal, 244, 33-43.

Seville, J.P.K., Ingram, A., Fan, X., Parker, D.J., 2009. Chapter 4 Positron Emission Imaging in Chemical Engineering. Adv. Chem. Eng. 37, 149–178.

Stein, M., Martin, T.W., Seville, J.P.K., McNeil, P.A., Parker, D.J., 1997. Positron emission particle tracking: Particle velocities in gas fluidised beds, mixers and other applications. Non-Invasive Monit. Multiph. Flows 309–333.

Tebianian, S., Dubrawski, K., Ellis, N., Cocco, R.A., Hays, R., Karri, S.B.R., Leadbeater, T.W., Parker, D.J., Chaouki, J., Jafari, R., Garcia-Trinanes P., Seville J.P.K. and Grace J.R., 2015. Investigation of particle velocity in FCC gas-fluidized beds based on different measurement techniques. Chem. Eng. Sci. 127, 310–322.

Tebianian, S., Dubrawski, K., Ellis, N., Cocco, R.A., Hays, R., Karri, S.B.R., Leadbeater, T.W., Parker, D.J., Chaouki, J., Jafari, R., Seville J.P.K. and Grace J.R, 2016a. Comparison of particle velocity measurement techniques in a fluidized bed oper.ating in the square-nosed slugging flow regime. Powder Technol. 296, 45–52.

Tebianian, S., Dubrawski, K., Ellis, N., Cocco, R.A., Hays, R., Karri, S.B.R., Leadbeater, T.W., Parker, D.J., Chaouki, J., Jafari, R., Garcia-Trinanes P, Seville JPK and Grace JR, 2016b. Solids flux measurements via alternate techniques in a gas-fluidized bed. Chem. Eng. J. 306, 306–321.

Vashisth, S., Ahmadi Motlagh, A.H., Tebianian, S., Salcudean, M., Grace, J.R., 2015. Comparison of numerical approaches to model FCC particles in gas–solid bubbling fluidized bed. Chem. Eng. Sci. 134, 269–286.

Verma, V., Li, T., Dietiker, J.F. and Rogers, W.A., 2016. Hydrodynamics of gas–solids flow in a bubbling fluidized bed with immersed vertical U-tube banks. Chemical Engineering Journal, 287, 727-743.

Verma, V., Li, T. and De Wilde, J., 2017. Coarse-grained discrete particle simulations of particle segregation in rotating fluidized beds in vortex chambers. Powder Technol. 318, 282-292.

Xu, Y., Li, T., Lu, L., Tebianian, S., Chaouki, J., Leadbeater, T.W., Jafari, R., Parker, D.J., Seville, J., Ellis, N., Grace, J.R., 2019a. Numerical and experimental comparison of tracer particle and averaging techniques for particle velocities in a fluidized bed. Chem. Eng. Sci. 195, 356–366.

Xu, Y., Gao, X., Li, T., 2019b. Numerical study of the bi-disperse particles segregation inside a spherical tumbler with Discrete Element Method (DEM). Comput. Math. with Appl.

Xu, Y., Musser, J., Li, T., Gopalan, B., Panday, R., Tucker, J., Breault, G., Clarke, M.A. and Rogers, W.A., 2018. Numerical Simulation and Experimental Study of the Gas–Solid Flow Behavior Inside a Full-Loop Circulating Fluidized Bed: Evaluation of Different Drag Models. Industrial & Engineering Chemistry Research, 57(2), 740-750.

Xu, Y., Li, T., Musser, J., Liu, X., Xu, G., Rogers, W.A., 2017a. CFD-DEM modeling the effect of column size and bed height on minimum fluidization velocity in micro fluidized beds with Geldart B particles. Powder Technol. 318, 321-328.

Xu, Y., Musser, J., Li, T., Padding, J.T., Rogers, W.A., 2017b. Particles climbing along a vertically vibrating tube: numerical simulation using the Discrete Element Method (DEM). Powder Technol. 320, 304–312.

Xu, Y., Padding, J.T., Kuipers, J.A.M., 2014. Numerical investigation of the vertical plunging force of a spherical intruder into a prefluidized granular bed. Phys. Rev. E 90, 062203.

Xu, Y., Padding, J.T., van der Hoef, M.A., Kuipers, J.A.M., 2013. Detailed numerical simulation of an intruder impacting on a granular bed using a hybrid discrete particle and immersed boundary (DP-IB) method. Chem. Eng. Sci. 104, 201–207.